Design of a Boron-Doped Diamond Microcell Grafted with HRP for the Sensitive and Selective Detection of Ochratoxin A

Amani Chrouda, Dhekra Ayed, Manahil Babiker Elamin, Shazalia Mahmoud Ahmed Ali, Laila M Alhaidari, Francois Bessueille, Nicole Jaffrezic-Renault

chemosensors

MDPI

Article

Design of a Boron-Doped Diamond Microcell Grafted with HRP for the Sensitive and Selective Detection of Ochratoxin A

Amani Chrouda [1], Dhekra Ayed [2], Manahil Babiker Elamin [1,*], Shazalia Mahmoud Ahmed Ali [1], Laila M. Alhaidari [1], Francois Bessueille [3] and Nicole Jaffrezic-Renault [3,*]

[1] Department of Chemistry, College of Science at Zulfi, Majmaah University, Zulfi 11932, Saudi Arabia
[2] Laboratory of Interfaces and Advanced Materials, Faculty of Sciences, University of Monastir, Monastir 5019, Tunisia
[3] Institute of Analytical Sciences, University of Lyon, UMR CNRS-UCBL 5280, 5 Rue la Doua, 69100 Villeurbanne, France
* Correspondence: m.elamn@mu.edu.sa (M.B.E.); nicole.jaffrezic@univ-lyon1.fr (N.J.-R.)

Abstract: Ochratoxin A (OTA) is considered the most toxic member of the ochratoxin group. Herein, a novel label-free electrochemical sensor based on the horseradish peroxidase (HRP) enzyme is developed for OTA detection. The HRP enzyme was covalently immobilized on the working electrode of a planar boron-doped diamond (BDD) electrochemical microcell previously covered with diazonium film and grafted with single-walled carbon nanotubes (SWCNTs). Each surface modification step was evaluated by cyclic voltammetry and scanning electron microscopy. Square wave voltammetry was used for the detection of OTA. The linear working range of the biosensors ranged between 10^{-14} and 0.1 M, with a limit of detection (LOD) of 10 fM, an RSD equal to 5%, and a sensitivity of 0.8 µA per decade. In addition, the sensor showed good selectivity in the presence of OTA analogs; it was validated in samples such as corn, feed, and wheat. The metrological performance of the present sensor makes it a good alternative for OTA detection.

Keywords: ochratoxin A; boron doped diamond microcell; horseradish peroxidase; electrochemical biosensor

Citation: Chrouda, A.; Ayed, D.; Elamin, M.B.; Ali, S.M.A.; Alhaidari, L.M.; Bessueille, F.; Jaffrezic-Renault, N. Design of a Boron-Doped Diamond Microcell Grafted with HRP for the Sensitive and Selective Detection of Ochratoxin A. *Chemosensors* **2023**, *11*, 176. https://doi.org/10.3390/chemosensors11030176

Academic Editor: Xiaobing Zhang

Received: 25 January 2023
Revised: 23 February 2023
Accepted: 1 March 2023
Published: 5 March 2023

1. Introduction

Ochratoxin A (OTA) is one of the mycotoxins produced by strains of *Penicillium* and *Aspergillus*. OTA is highly toxic to human and animal bodies. It can enter the body through the digestive or respiratory tracts or through the skin [1]. Moreover, OTA can cause different forms of kidney, brain, and liver diseases. At present, OTA could exist in any species in agricultural areas; it is widely found in many products such as beans, cereals, grape juice, coffee, wine, and dried fruit [2]. Moreover, OTA is chemically stable and can survive in harsh conditions such as high temperatures and boiling. Thus, OTA is difficult to eradicate from food. Therefore, governments have set strict restrictions on the content of ochratoxin A in food. The European Commission has set a maximum tolerated OTA concentration of 2 ppb in juices and wine and 5 ppb in cereals [3].

Up to now, conventional methods used for OTA detection have been largely concentrated in advanced instrumental techniques such as ELISA [4], high-performance chromatography (HPLC) [5], immunochromatography [6], and high-performance thin-layer chromatography [7]. Although these methods are highly sensitive and selective, with the limit of detection being in the range of ng/mL, there are still inescapable drawbacks, such as the long time required for preparation, the high cost, and the strict experimental conditions. To avoid these problems, electrochemical biosensors for OTA detection are the subject of intensive research. They appear to be promising tools because of their simplicity, low cost, high sensitivity, and miniaturization. Several designs of electrochemical biosensors for OTA detection were published to take up the challenges [8–10]. The unique

combination of OTA with recognition elements is vital to the construction of OTA electrochemical biosensors. Aptamers [9], antibodies [11], and molecularly imprinted polymers (MIPs) [12] play an important and major role in the sensor construction. According to recent studies, a primary imperfection of the biosensors based on antibody applications is due to the irreversibility of the formation of the antibody-OTA complex, thereby limiting the shelf life of the immunosensor. The typical shelf life of the published immunosensors is two weeks [11,13]. Moreover, the acquisition procedure of antibodies with OTA is usually expensive, time-consuming, and depends on immunization with little success [8]. On the other hand, the selectivity of molecularly imprinted polymers (MIPs) is insufficient to compete with recognition receptors [14], and their shelf life is also limited at less than two weeks [12]. There is still a worry about the application of aptamers in OTA sensors; although these strategies are quite attractive due to the selectivity of aptamers and their robustness, they still suffer from costly amplification processes that greatly hinder their commercial potential. The reversibility of the aptamer-OTA complex is quite limited, and the shelf life of the aptasensors is two weeks or less [15–17]. To avoid the aforementioned problems, it is of great importance to develop and explore other types of recognition elements. Enzyme-assisted target molecule recovery technologies provide a feasible strategy for OTA detection. Furthermore, few enzymatic electrochemical biosensors for OTA detection have been developed; the high interest in enzyme applications stems from their reversibility.

The reduction in OTA levels in food products can be obtained by enzymes able to cleave the OTA molecules into non-toxic molecules: carboxypeptidase A and Y [18–20] or other hydrolases, such as lipases [21,22], proteases [22,23], and ochratoxinase [23]. These enzymes are also good candidates for the recognition part of biosensors. Carboxypeptidase Y (CPY), a serine-type carboxypeptidase [24], was used for the detection of OTA with a conductometric transducer after CPY immobilization through cross-linking on interdigitated electrodes [25]. This enzyme is able to cleave the OTA molecule at the amide bond connecting L-b-phenylalanine to the OTA moiety, according to Equation (1).

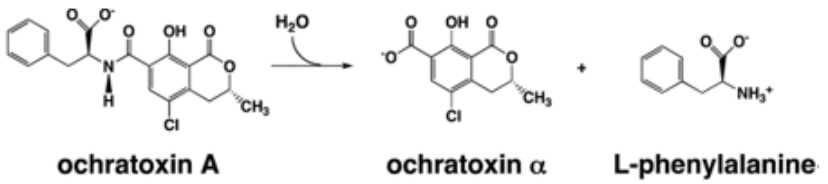

(1)

For its part, thermolysin (TLN) is a neutral Zn^{2+}-metalloendopeptidase produced by Bacillus thermoproteolyticus [26]. Peptide bonds are specifically cleaved by TLN at the N-terminus of hydrophobic residues such as leucine and phenylalanine [27], as in equation 1. It was used in a conductometric biosensor [26,28] and in an impedimetric biosensor [29]. Very comparable Michaelis–Menten constants were obtained for CPY and TLN-based conductometric biosensors, 25 µM and 26 µM respectively [26,28]. For the impedimetric biosensor, where TLN was immobilized on GCE modified with AuNP-decorated graphene, the concentration was found to be in the order of nM [30]. It is known that the activity of immobilized enzymes can be very low compared to that of the free enzyme. In the case of free thermolysin, its concentration is in the range of mM [26]; when TLN is immobilized, this value is observed to decrease. The simple Michaelis-Menten model should not be applicable when TLN is immobilized due to diffusion terms [28].

HRP, a ferric enzyme, can initiate its catalytic cycle by rapid oxidation by H_2O_2 via a heme-oxygen complex as oxidized forms of the native enzyme heme via the formation of compound I (Equation (2)) [29,31].

$$HRP + H_2O_2 \rightarrow \text{compound I } [(Fe(IV)=O)P^{\bullet+}] + H_2O \quad (2)$$

In contact with an electron donor substrate S, the compound I returns to its resting state through two successive single electron transfer reactions. Different electron donor substrates can be involved in this electron transfer, and the oxidized S is then detected through voltammetry: 4-tert-butylcatechol, dopamine [32], phenolic compounds [33], and rifampicin [34]. The phenolic function of ochratoxin is an electron donor substrate, and after its oxidation [35], it can be detected by its reduction at a screen-printed electrode, as proposed by Alonso-Lomillo [36,37]. The amperometric detection is obtained by the reduction of the 1,4-benzoquinone group of the oxidized OTA at −180 mV [38] (Figure 1).

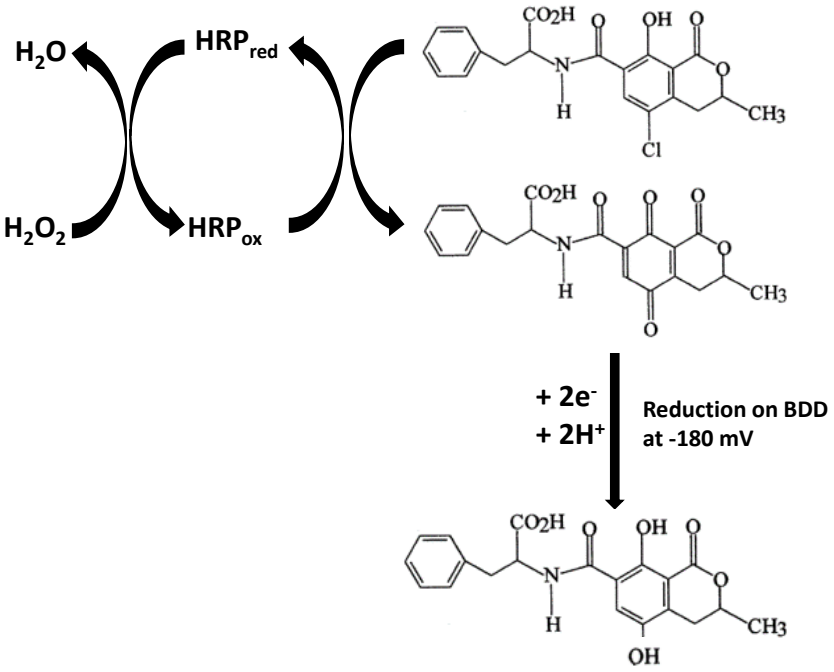

Figure 1. Mechanism of OTA oxidation by the oxidized HRP enzyme and of the origin amperometric signal.

On the other hand, the use of modern sensitization technology in the signal transducer is greatly important to enhance sensor performance. Therefore, single-walled carbon nanotubes (SWCNTs) could be used as bridges to connect biomolecules to the electrode surface. They could also be used to accelerate the electron transfer rate at interfaces. Among the transducer surfaces that have gained considerable interest in sensor technology, boron-doped diamond (BDD) film is selected as a transducer surface. BDD electrodes present many outstanding properties, such as excellent mechanical properties, a wide electrochemical potential window (from −1.35 V to 2.3 V) in aqueous electrolytes, high response reproducibility, and a stable capacitive background current [11,15].

In the present work, a novel electrochemical biosensor for OTA trace-level detection is elaborated. For the first time, OTA is detected using a reversible enzymatic system based on HRP and linked to a high transfer rate transduction system composed of a BDD electrode modified with SWCNTs. Moreover, the BDD electrode is included in a three-electrode BDD microcell inserted in a wall-jet flow cell, leading to a miniaturized analytical system for rapid OTA detection, requiring less than three minutes for one measuring point. The proposed new OTA biosensor is constructed by the grafting of the horseradish peroxidase enzyme (HRP) into SWCNT surfaces, covering the working electrode of a planar Boron Doped Diamond (BDD) microcell. The connection of HRP and SWNCT allows the immobilization of a high density of HRP and its availability for interaction with H_2O_2 and with OTA molecules in the solution. Cyclic voltammetry (CV) and electrochemical impedance spectroscopy were used to characterize and investigate each surface modification step and the OTA binding process. As the biosensor response,

the reduction signal of the oxidized OTA was measured using square wave voltammetry. This electrochemical OTA biosensor was then successfully tested in real samples such as corn, feed, and wheat.

2. Materials and Methods

2.1. Chemicals

SWCNTs functionalized with-COOH were prepared by the HiPco process and purchased from Carbon Nanotechnologies Inc. (Houston, TX, USA). Ochratoxin A, sulfuric acid, potassium chloride, ethanol, acetone, hydrochloric acid, potassium chloride, potassium ferricyanide, 4-phenylenediamine, and horseradish peroxidase (HRP) were purchased from Sigma-Aldrich (Saint-Quentin-Fallavier, France). N-hydroxysuccinimide (NHS), 1-ethyl-3-(3dimethylaminopropyl)-carbodiimide hydrochloride (EDC), ethanol, and acetone were purchased from Thermo-Fisher (Illkirch-Graffenstaden, France). All available reagents were used without further purification. All solutions were prepared with double-ionized water (having a resistivity of 18.2 MΩ). The PH value of the phosphate buffer solution (PBS) used in this work was adjusted at 7.0.

2.2. BDD Electrochemical Microcell

An electrochemical microcell was obtained using a microcrystalline BDD film (300 nm) deposited on a silicon wafer, provided by NeoCoat SA (La Chaux-de-Fonds, Switzerland). The polycrystalline BDD film with a boron concentration higher than 8000 ppm was obtained by microwave-assisted plasma-enhanced chemical vapor deposition (MPECVD) on an insulating layer of silicon oxide and silicon nitride ($Si/SiO_2/Si_3N_4$) with a thickness of 0.5 microwave-assisted plasma-enhanced chemical vapor deposition (MPECVD) on an insulating layer of silicon oxide and silicon nitride ($Si/SiO_2/Si_3N_4$) with a thickness of 0.5 mm. The three electrodes, the counter electrode, the working electrode, and the reference electrode, were cut out of the BDD film by micromachining (Figure 2). This was done using a femtosecond laser (5 kHz, 2.5 W, 800 nm, and 150 fs) by MANUTECH USD (Saint-Etienne, France).

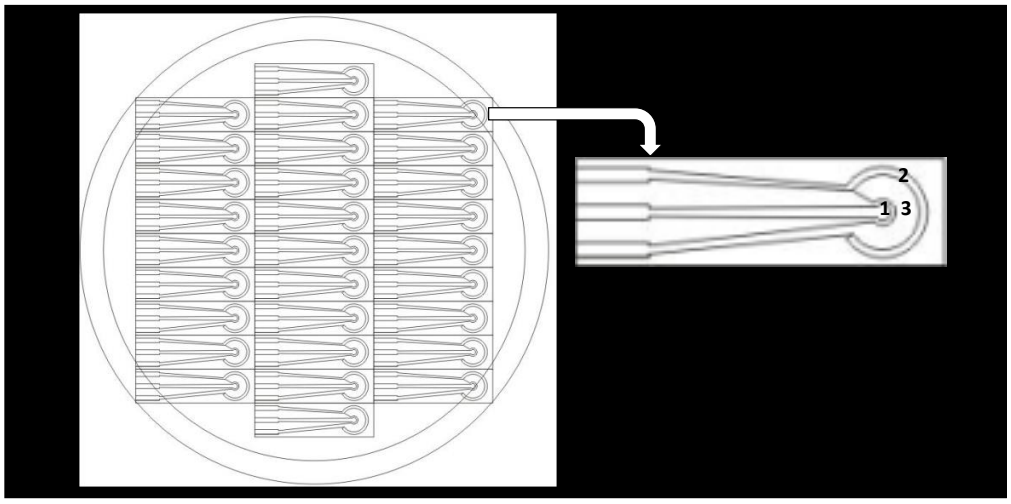

Figure 2. Scheme of a 4 inch silicon wafer covered with a polycrystalline BDD film (500 μm thick), micromachined using a femtosecond laser into 29 BDD microcells and of one BDD microcell including the working electrode (1), the counter electrode (2), and the pseudo reference electrode (3). Copyrights from Elsevier [39].

2.3. Surface Modification of BDD

The BDD microcells were cleaned and activated by 10 mL of Piranha solution for 5 min. The BDD microcells were then rinsed with distilled water and dried under a nitrogen flow. After cleaning, the 4-phenylenediamine was diazotated in an aqueous solution containing

20 mM HCl and 20 mM $NaNO_2$ for 10 min, under stirring at 0 °C. Diazonium salt (DS) was directly deposited on the BDD working electrode surface by electro-addressing, then potential was scanned from 0.6 to −400 mV at a scan rate of 100 mV/s.

The carboxylic group of SWCNTs-COOH (1 mg/mL) was activated in the presence of 20.6 mg of EDC and 11.5 mg of NHS in 1 mL of DMSO for 30 min. Then, activated SWCNTs-COOH were dispersed in a 0.1 M carbonate buffer, pH 11, containing HRP (10 g/mL), and injected in the flow cell, in contact with the DS-functionalized BDD surface, for 2 h. After reaction, the surface was rinsed with 0.1 M PBS.

2.4. Electrochemical Measurements

Cyclic voltammetry (CV) and square wave voltammetry (SWV) measurements were carried out with an Autolab PGSTAT (AUT 83965) potentiostat/galvanostat system controlled by the Autolab software NOVA 1.5 (Metrohm, Herisau, Switzerland). Electrochemical measurements were performed at room temperature (25 °C). Experiments were performed using a 5 µL wall-jet flow cell provided by BVT Technology (Stráek, Czech Republic). The electrical contact is obtained by applying pressure to the BDD electrode's front side.

For the electrochemical impedance spectroscopy (EIS) measurements, an alternative potential of low amplitude (5 mV) was used, in (10 mHz–100 kHz) frequency domain.

OTA samples were prepared in 0.1 M PBS with 1 mM H_2O_2. Square-wave voltammetry measurements (100 mV/s, Estep = 0.01 V, and frequency = 25 kHz) were conducted in a potential range of 0.1 to −0.4 V. Electrochemical measurements were triplicated for each OTA concentration. Less than 3 min for one measuring point.

2.5. Scanning Electron Microscopy (SEM) Measurements

Scanning electron microscopy (SEM) images were obtained using a VEGA TESCAN SEM.

2.6. Contact Angle Measurements

The contact angle measurements were carried out to measure the surface energy of the functionalized electrodes by using a Digidrop contact angle instrument (GBX Scientific Instrument, Romans, France). The measurement was assessed by the deposition of 2 mL of distilled water on each sample surface using a drop of water from an adapted syringe in air at room temperature. By adopting the tangent method, the contact angle was determined on both sides of the drops.

2.7. FTIR

FTIR analyses were monitored using a Perkin Elmer "Spectrum 2" spectrometer connected to an attenuated total reflectance cell (ATR). Spectra were recorded at room temperature from 500 to 4000 cm^{-1} with a resolution of 2 cm^{-1}.

2.8. Analysis of the Real Samples and LC-MS/MS Measurements

To investigate the potential of the designed sensor to detect Ochratoxin A in real samples, three dry commercial samples of corn, wheat, and feed stuff, were analyzed using standard addition method, in triplicate. Samples were extracted and cleaned according to Rahman et al. (2010) [40]. The samples were ground to a powder, using a blender. The powder (20 g) was weighed. Then, 100 mL of acetonitrile/water (60:40, v/v) solution was added, and the solution was stirred for 60 min. After centrifugation at 3000 rpm for 15 min, the supernatant was passed through a 0.45-nm membrane filter, and 10 mL of the filtrate was diluted with 40 mL of Phosphate Buffered Saline (PBS). A total of 10 mL of the diluted extract was passed through immunoaffinity columns (IAC) at a flow rate of about 2–3 mL per min. The column was washed with 10 mL of PBS followed by 10 mL of water and OTA was eluted with 3 mL of methanol into a vial at a flow rate of one drop/s. Then the eluate was evaporated to dryness under a gentle stream of nitrogen at 50 °C. The residue was

re-dissolved in 500 mL methanol/water (50:50, v/v) and finally, 50 mL of the aliquot was analyzed with the sensors and 50 mL of the aliquot was injected into the Agilent 6475 triple quadrupole LC-MS/MS system.

3. Results and Discussion

3.1. Biosensor Design

Functionalization of the electrode surface is a vital step in biosensor design. The most straightforward approach is the recovery of the surface with polymers richer in functional groups. Given its versatility, uncomplicated functionalization procedure, stability, biocompatibility, and richness of functional groups, the diazonium salt (DS) is selected as a functional monomer for surface modification [41]. As presented in Figure 3a, the diazonium salt is first electropolymerized on the BDD surface using cyclic voltammetry. Figure 3b presents the voltammograms of DS electropolymerization. A broad irreversible reduction peak appears in the first cycle, at approximately −0.1 V vs. Ag/AgCl [42]. This irreversible peak is attributed to the formation of the DS radical, which can form a covalent metal-carbon bond with the BDD surface [42]. The subsequent decrease in the current peak indicates the formation of a semi-permeable layer on the electrode surface [42]. Due to interesting properties such as sensitivity, selectivity, the ability to measure very small concentrations, and physical and chemical stability, nanotechnology in general and carbon nanotubes (CNTs) in particular are becoming the most used in sensor surface modification [43]. For these reasons, the BDD surface recovered with DS film was modified with functionalized single-walled carbon nanotubes (SWCNTs). The final step then consists of covalently grafting the HRP enzyme onto the activated acid groups with the EDC/NHS couple.

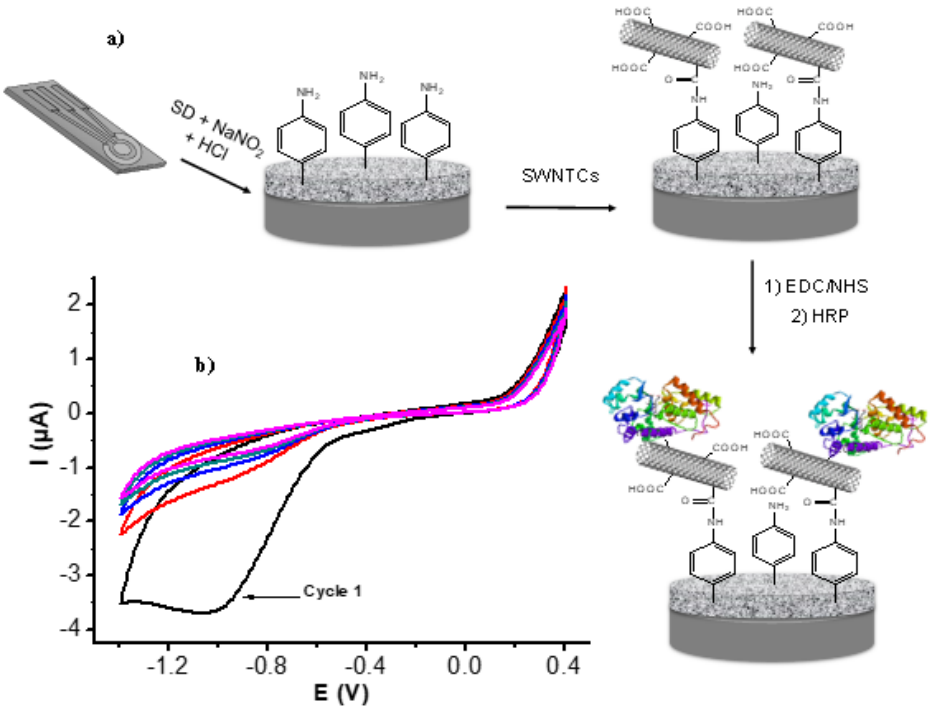

Figure 3. (**a**) Schematic illustration of the different steps of the biosensor fabrication; (**b**) Cyclic voltammograms of DS electropolymerization.

3.1.1. Electrochemical Characterization

The different steps of surface modification were monitored using electrochemical methods. The distinct voltammograms, illustrated in Figure 4, demonstrate the conductive nature of the electrode surface after each step of surface modification.

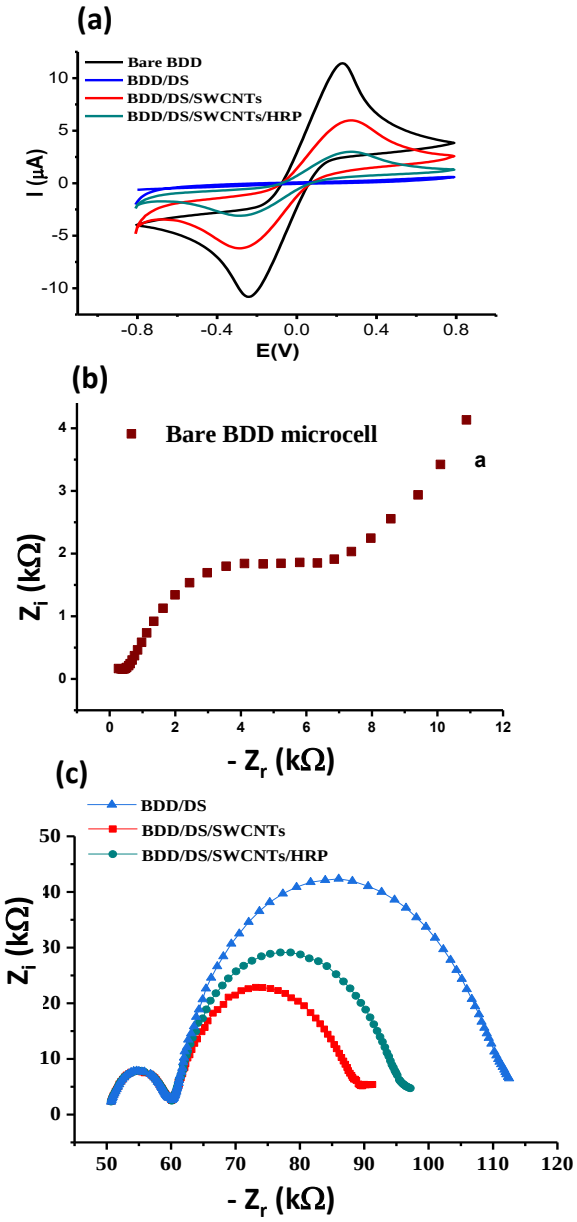

Figure 4. (**a**) Cyclic voltamograms, and (**b**,**c**) Nyquist plots obtained after the different steps of fabrication of the biosensor: Bare BDD (black curve), BDD-SD (red curve), BDD-SD-SWCNTs (blue curve), and BDD-SD-SWCNTs-HRP (green curve) Measuring media: 0.1 M of PBS with 5 mM of Fe^{3+}/Fe^{2+} probe.

In Figure 4a, the reversible voltammogram of the bare BDD surface (black curve) indicates its good conductivity. Following the DS polymer formation on the surface, an important decrease in current density was observed. This variation could be attributed to the formation of the DS resistive film on the BDD surface, which minimizes electron transfer. This phenomenon was already visualized by Lo et al. [44]. Interestingly, the surface modification with SWCNTs significantly increased the redox peak current. This charge transfer enhancement could be attributed to the homogenous distribution of SWCNTs on the BDD-DS surface [45]. This distribution expands the electroactive area, which increases the absorption capacity of the electroactive probe. However, the covalent attachment of the HRP enzyme to the BDD surface decreases the current density transfer. This variation could be attributed, on the one hand, to the steric hindrance provided by the large weight of HRP. On the other hand, it was anticipated that the negatively charged HRP groups,

such as hydroxyl and acid groups, would resist the redox probe, thereby minimizing the charge transfer.

Electrochemical impedance spectroscopy (EIS) was used to characterize the different steps of the electrode modification. The Nyquist plot for bare BDD (Figure 4b) presents a very small semicircle with a straight Warburg line, which suggests a low electron transfer resistance to the redox probe at high frequencies and a semi-infinite diffusion phenomenon at low frequencies. In Figure 4c, the semicircle, in the high frequency range, is attributed to the DS film. Its diameter did not change after the next steps of electrode modification. The increase in diameter of the low-frequency semicircle after surface modification with DS film could be explained by the increase in interfacial charge transfer resistance. The DS modification with SWCNTs decreases the charge transfer, reflecting the enhancement of redox probe charge transfer by increasing the surface area and the interface conductivity. After the HRP protein immobilization, the Rct increases, which could be attributed to the formation of the insulating protein layer. The results obtained are in good agreement with those obtained using CV measurements.

3.1.2. Morphological Characterization

SEM was used to analyze the morphology of the transducer surface after all modifications (Figure 5). The SEM image of the bare BBD surface (Figure 5A) exhibits the crystalline structure of BDD. SEM image of BDD, SD, SWCNTs, and HP (Figure 5B) shows the filamentous structure of SWCNTs covering the whole surface.

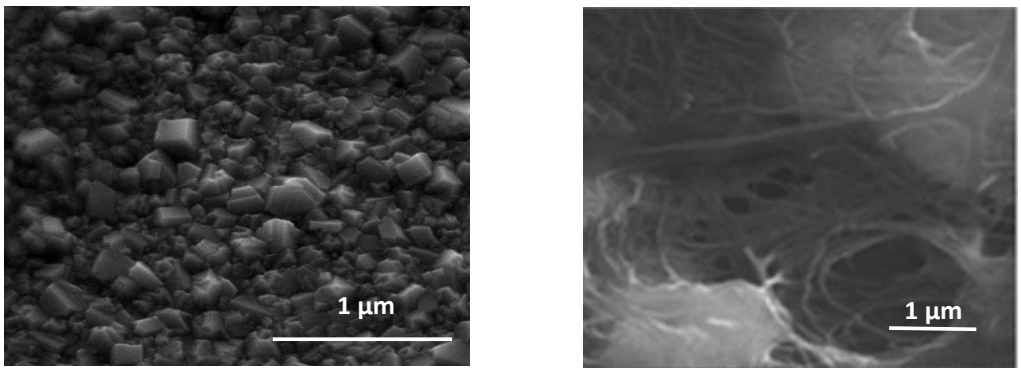

Figure 5. (**A**) SEM image of bare BDD; (**B**) SEM image of BDD/SD/SWCNTs/HRP.

3.1.3. FTIR and Contact Angle Characterization

The FTIR spectra in Figure 6a show the appearance of absorption peaks at 1627.8 cm^{-1} and 3440.8 cm^{-1}, which are most likely the characteristic peaks of the acid groups COOH of the SWCNT matrix. These hydrophilic groups are probably responsible for the decrease in the angle of contact, visualized on Figure 6b, from 77.4° to 25.4°. The collected FTIR data as well as the contact measurements confirm the BDD surface modification with the functionalized SWCNTs. In the free HRP spectrum (red curve), a broad and strong NH_3 stretching band in the 2950–2600 cm^{-1} region is observed as the characteristic of amino acids. The absorption peaks at 1661 cm^{-1} and 1529 cm^{-1}, respectively, to the Amide I and Amide II bands of HRP. The absence of COOH peaks in the BDD/DS/SWCNTs spectrum (blue curve) indicates the formation of amide bonds between HRP amine groups and SWCNT carboxyl groups, and the presence of HRP Amide I and Amide II bands in the BDD/DS/SWCNTs spectrum confirms the covalent immobilization of HRP protein to the functionalized SWCNTs matrix.

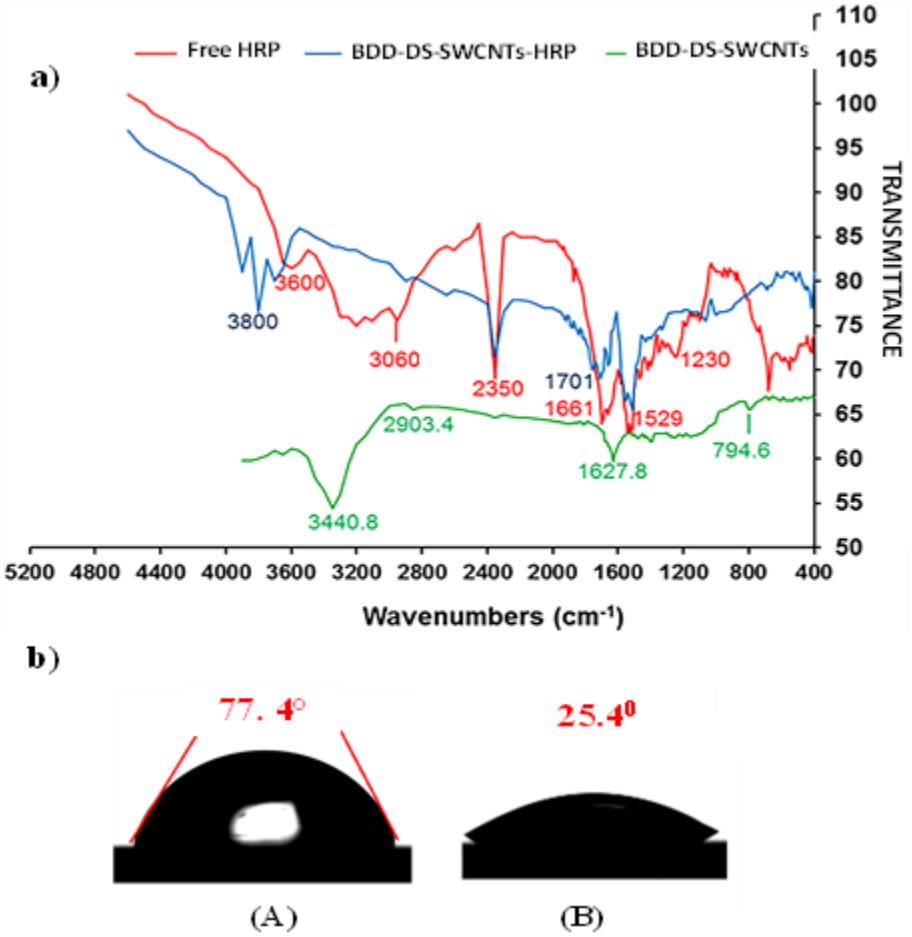

Figure 6. (**a**) FTIR spectra for free HRP, BDD/DS/SWCNTs and BDD/DS/SWCNTs/HRP, (**b**) angle of contact measurements of BDD surface (**A**) before and (**B**) surface modification with SD-SWCNTs.

3.2. Analytical Performance of the HRP Biosensor

3.2.1. SWV Response of the HRP-Based Sensor

The SWV response of the HRP-based sensor was then investigated for a wide range of OTA concentrations in solution. According to the results shown in Figure 7, the catalytic oxidation peak of OTA appeared at −180 mV, and the peak current increases as the OTA concentration increases from 10^{-14} M to 10^{-1} M. This variation confirms the capacity of HRP to oxidize OTA, and its reduction is observed at the same potential as that of 4-*tert*-butyl-*o*-benzoquinone [45].

To evaluate the HRP-based sensor performance, merit parameters, including reproducibility, limit of detection, and sensitivity, were determined. Therefore, the variations of intensity of the SWV peak maximum versus log concentration of OTA are presented in Figure 8. Measurements were carried out in triplicate. Results demonstrated good reproducibility with a relative standard deviation (RSD) of 5%. The equation of the calibration curve in the low concentration range is: I (μA) = 0.8 log[OTA]—12.1 with a linear correlation coefficient R^2 equal to 0.97. The limit of detection is determined according to the formula 3 s/S, s being the background of the blank and S being the sensitivity. It is found to be 10 fM. The estimated Michaelis-Menten constant, calculated from the concentration at Vmax/2, should be 10 pM. This very low value shows the high availability of HRP for interaction with OTA molecules.

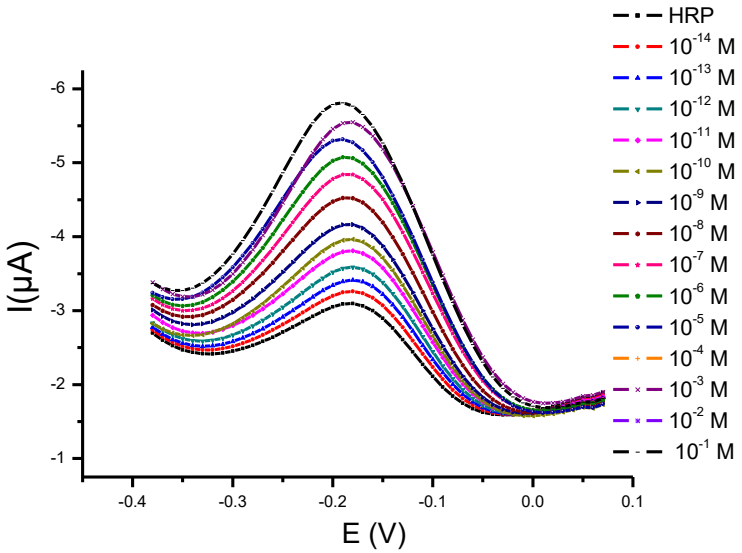

Figure 7. SWV voltammograms for different OTA concentrations. All measurements are recorded in 0.1 M of PBS with 1 mM H_2O_2.

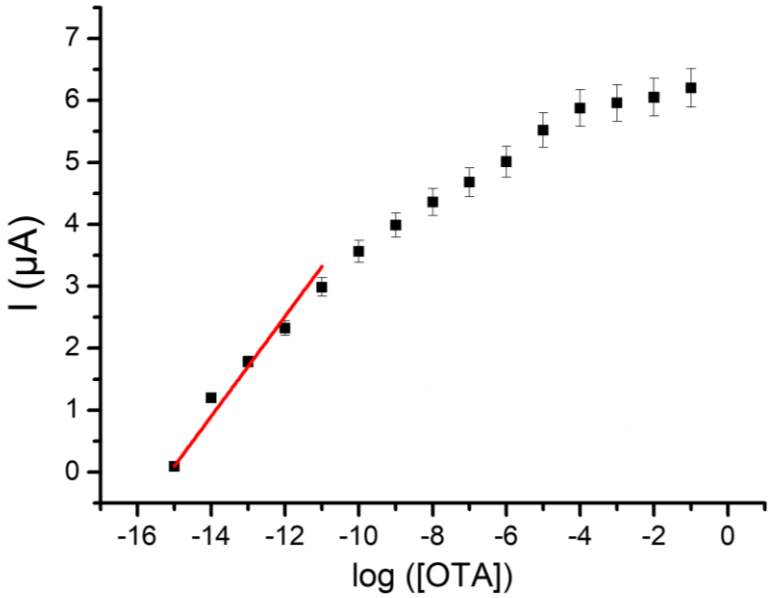

Figure 8. Calibration curve of the HRP sensor versus log OTA concentration.

To highlight the contribution of the present work, the recent publications about OTA detection using natural receptors such as antibodies and artificial receptors, including aptamers and molecularly imprinted polymers (MIPs), are presented in Table 1. When compared to immunosensors, aptasensors, and MIP-sensors, the current work has the lowest detection limit and the widest detection range. Although these entities could minimize the non-specific interactions, they present many drawbacks, such as degradation over time [46], recyclability, difficulty of preparation [46], and especially the high cost [47]. Sensor-based HRP could be considered an appropriate alternative to aptasensors for specific and selective OTA detection.

Table 1. Recently published sensors for OTA detection: immunosensors, aptasensors, MIP-based sensors, and enzymatic sensors.

	Sensor Design	Detection Range ng/mL	Real Sample	LOD ng/mL	Refs
Antibodies	BSA/anti-OTA/PdNPs/SPCEs	0.3–8.5	wheat	0.86	[48]
	BSA/anti-OTA/PdNPs/CF	0.5–20	coffee	0.096	[13]
	Anti-OTA-MNPs/BSA/GA/TA/Au	0.01–5	wine	0.01	[49]
	Anti-OTA/DIA/BDD	7–25	coffee	7×10^{-3}	[11]
Aptamers	Apt/PEG/BDD	0.01–13.2	coffee	0.01	[15]
	MB/Cas-cDNA/Apt/Au	0.10–10	corn	0.1×10^{-3}	[50]
	Th-cDNA-Bio-Apt/SA-Gr/GCE	0.01–5	beer	0.13×10^{-3}	[16]
	Apt/DNA1/DNA2/Ch/Hyd/CGE	0.1–100	wine	0.03	[17]
	Apt/Ch-MoS2-Au@Pt/PAD	0.1–200	corn	25.2×10^{-6}	[51]
	Thi/HRP-DNA/DSN/Zif-8-AuNPs/ITO	$(1–107) \times 10^{-6}$	wheat	247×10^{-6}	[52]
	MB/Apt/6-MHOH/Au	0.1–300	coffee beer	78.3×10^{-3}	[53]
MIP	CGE/MWCNTs/MIP	$(20.19–403.8) \times 10^{3}$	beer wine	1.7×10^{-3}	[12]
Enzyme	HRP/SPE	$(9.63–82.08) \times 10^{3}$	beer	10.8	[37]
	HRP/Ppy/SPCEs	$(0.09–1.05) \times 10^{3}$	beer coffee	0.04	[36]
	CPY/BSA/IDT TLN/BSA/IDT	$(0.40–30.28) \times 10^{3}$	olive oil	1×10^{3}	[25]
	TLN/AuNPs/(PVA/PEI)/IDT	$(0.40–24.22) \times 10^{3}$	olive oil	0.4	[28]
	TLN/AuNPs/CCLC/GR/GCE	$(0.08–40.38) \times 10^{3}$	coffee	80.8×10^{-3}	[30]
	HRP/MWNTs/DS/BDD	4.04×10^{-3}–4.04×10^{-8}	corn, wheat, feed stuff	4.04×10^{-6}	The present work

Apt: aptamer; BSA: bovine serum albumin; Cas: Carbon aerogels; CCLC: calcium cross-linked cellulose; Ch: Chitosan; CF: Carbon felt; CPY: Carboxypeptidase Y; DIA: diazonium; Hyd: Hydrogel; GA: Glutaraldehyde; Gr: Graphen; IDT: interdigitated electrodes; MB: Methyleneblue; 6-MHOH: 6-mercaptohexanol; MNPs: magnetic nanoparticles; PAD: paper-based analytical device; PdNPs: Palladium nanoparticles; PEG: polyethylene glycol; Ppy: polypyrrole; SA: streptavidin; TA: 11-amino-1-undecanethiol; TLN: Thermolysin; TA: Thiolamine; Thi: Thionine; ZIF: zeolite imidazole framework.

Only Alonso-Lomillo et al. elaborated a HRP-based sensor for OTA detection [36,37]. The biosensor was designed by HRP enzyme physical adsorption on screen-printed carbon electrodes (SPCE). The limit of detection found by this team is from 0.1 nM to 26.77 nM, these values are higher than the LOD found in the present work. This difference may be attributed to the covalent attachment of HRP on SWCNTs surface, ensuring a high density of grafted and dispersed HRP.

Comparing the limit of detection of the present biosensor to that of the conventional methods, which is in the range of ng/mL, it comes out that it is one million times lower.

Long-term storage stability was also studied. Three different HRP sensors were fabricated, and their responses were measured every day for 30 days. After each test, HRP sensors were rinsed with UPW and stored at +4 °C in 20 mM phosphate buffer (pH 7). Only 10% of the initial response was lost after 15 days, and more than 85% remained after 30 days.

3.2.2. Selectivity Measurements

The selectivity of the OTA sensor was evaluated by evaluating its ability to discriminate between the target molecule (OTA) and interfering molecules such as ochratoxin B, aflatoxin B1, and aflatoxin M1. The selection of interfering molecules was based on their charge, molecular weight, and possible presence in real samples. The same concentration of each molecule was used: 1 mM.

Results, presented in Figure 9, show that HRP-based sensor sensitivity towards OTA is higher than that of interfering molecules: 3.6 times higher than ochratoxin B,

5.3 times higher than aflatoxin B1, and 21.5 times higher than aflatoxin M1. This sensor's cross-selectivity is similar to that shown in [54], where the aptasensor is five times more sensitive for OTA than for OTB, OTC, and OTB. The present sensor is able to discriminate perfectly between OTA and its analogue, ochratoxin B, when this analogue is in a lower concentration.

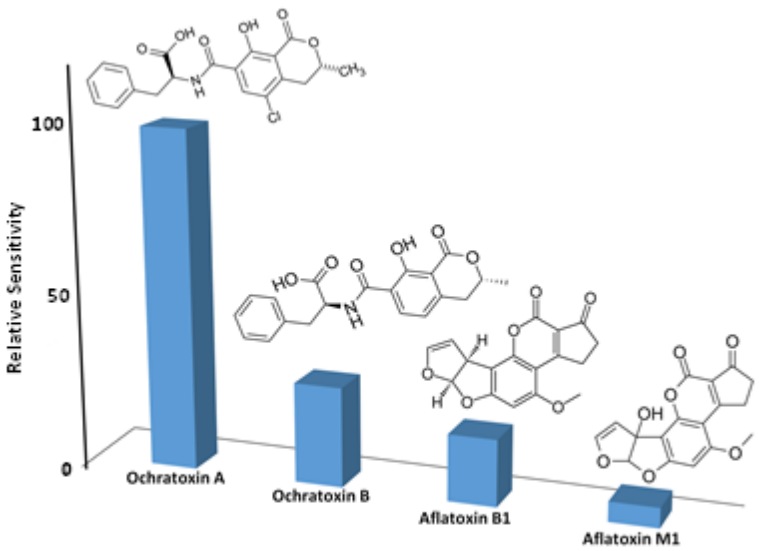

Figure 9. Sensitivity of the OTA sensor in the presence of Ochratoxin A, Ochratoxin B, Aflatoxin B1 and Aflatoxin M1.

3.2.3. Validation in Real Sample

To investigate the potential of the designed sensor to detect ochratoxin A in real samples, three dry commercial samples of corn, wheat, and feed stuff were analyzed using the standard addition method in triplicate. For analysis, samples were ground to a powder using a blender. The powder (20 g) was weighed. Then 100 mL of acetonitrile/water (60:40 v/v) solution was added, and the solution was stirred for 60 min. After centrifugation at 3000 rpm for 15 min, the supernatant was passed through a 0.45-nm membrane filter. The quantification of OTA was carried out with three different sensors using the standard addition method. The discovered values are correlated with those discovered by LC-MS/MS chromatography. The results, shown in Table 2, show a good correlation between both techniques, indicating that the designed sensor has a promising future application in real samples.

Table 2. Recovery of Ochratoxin A levels in corn, wheat, and feed using LC-MS/MS and the fabricated biosensor.

Samples	**HRP Biosensor (µg/kg),**		**LC-MS/MS (µg/kg), Mean ± SD**
	Mean ± SD	Recovery rate	
Corn	42.0 ± 1.9	84 ± 13%	50.0 ± 1.2
Wheat	38.0 ± 2.0	93 ± 5%	40.5 ± 2.1
Feed stuff	9.0 ± 1.1	100 ± 12%	9.0 ± 1.4

4. Conclusions

In this work, a new ultra-sensitive, highly selective, and reversible sensor-based horseradish peroxidase enzyme (HRP) for the detection of trace levels of ochratoxin A was elaborated. The HRP enzyme was covalently immobilized on the working electrode of a planar Boron Doped Diamond (BDD) electrochemical microcell previously covered with diazonium film and single-walled carbon nanotubes (SWCNTs). The proposed enzymatic

biosensor exhibited a wider linear range from 10^{-14} to 0.1 M, with a low limit of detection of 10 fM. It also exhibits excellent selectivity toward OTA molecules. Moreover, the enzymatic OTA biosensor was successfully validated for the detection of OTA molecules in real samples.

Author Contributions: Conceptualisation, A.C. and L.M.A.; Methodology, F.B. and L.M.A.; validation, L.M.A.; investigation, D.A. and S.M.A.A.; Writing—original draft preparation, S.M.A.A.; writing—review and editing, M.B.E.; N.J.-R.; project administration, S.M.A.A.; funding acquisition, A.C. All authors have read and agreed to the published version of the manuscript.

Funding: The authors extend their appreciation to the deputyship for Research & Innovation, Ministry of Education in Saudi Arabia for funding this research work through Project Number IFP-2022-45.

Institutional Review Board Statement: Not applicable.

Informed Consent Statement: Not applicable.

Data Availability Statement: Not applicable.

Conflicts of Interest: The authors declare no conflict of interest.

References

1. Monteoliva, M.; Rasero, F.S.; Gorgé, J.L.; Mayor, F. Ochratoxin A, a Toxic Metabolite produced by Aspergillus ochraceus Wilh. *Nature* **1965**, *205*, 498–499. [CrossRef]
2. Bui-Klimke, T.R.; Wu, F. Ochratoxin A and human health risk: A review of the evidence. *Physiol. Behav.* **2018**, *176*, 139–148. [CrossRef] [PubMed]
3. Schrenk, D.; Bodin, L.; Chipman, J.K.; del Mazo, J.; Grasl-Kraupp, B.; Hogstrand, C.; Hoogenboom, L.; Leblanc, J.C.; Nebbia, C.S.; Nielsen, E.; et al. Risk assessment of ochratoxin A in food. *EFSA J.* **2020**, *18*, e06113. [CrossRef]
4. Garg, K.; Villavicencio-Aguilar, F.; Solano-Rivera, F.; Gilbert, L. Analytical Validation of a Direct Competitive ELISA for Multiple Mycotoxin Detection in Human Serum. *Toxins* **2022**, *14*, 727. [CrossRef]
5. Oncu-Kaya, E.M. Development and validation of a SPE-UHPLC-fluorescence method for the analysis of ochratoxin A in certain turkish wines. *Maced. J. Chem. Chem. Eng.* **2019**, *38*, 161–170. [CrossRef]
6. Li, M.; Lu, W.Y.; Mao, Y.H.; Qiu, X.C.; Du, D.L. An enhanced immunochromatography assay based on gold growth on the surface of E. coli carrier for the simultaneous detection of mycotoxins. *Talanta* **2023**, *251*, 123798. [CrossRef]
7. Teixeira, T.R.; Hoeltz, M.; Einloft, T.C.; Dottori, H.A.; Manfroi, V.; Noll, I.B. Determination of ochratoxin A in wine from the southern region of Brazil by thin layer chromatography with a charge-coupled detector. *Food Addit. Contam. Part B Surveill.* **2011**, *4*, 289–293. [CrossRef]
8. Lv, L.; Wang, X. Recent Advances in Ochratoxin A Electrochemical Biosensors: Recognition Elements, Sensitization Technologies, and Their Applications. *J. Agric. Food Chem.* **2020**, *68*, 4769–4787. [CrossRef]
9. Zejli, H.; Goud, K.Y.; Marty, J.L. Label free aptasensor for ochratoxin A detection using polythiophene-3-carboxylic acid. *Talanta* **2018**, *185*, 513–519. [CrossRef] [PubMed]
10. Liu, N.; Ni, D.; Tan, Y.; Zhao, Z.; Liao, Y.; Wang, H.; Sun, C.; Wu, A. An ultrasensitive amperometric immunosensor for zearalenones based on oriented antibody immobilization on a glassy carbon electrode modified with MWCNTs and AuPt nanoparticles. *Microchim. Acta* **2017**, *184*, 147–153. [CrossRef]
11. Chrouda, A.; Sbartai, A.; Bessueille, F.; Renaud, L.; Maaref, A.; Jaffrezic-Renault, N. Electrically addressable deposition of diazonium-functionalized antibodies on boron-doped diamond microcells for the detection of ochratoxin A. *Anal. Methods* **2015**, *7*, 2444–2451. [CrossRef]
12. Pacheco, J.G.; Castro, M.; Machado, S.; Barroso, M.F.; Nouws, H.P.A.; Delerue-Matos, C. Molecularly imprinted electrochemical sensor for ochratoxin A detection in food samples. *Sens. Actuators B Chem.* **2015**, *215*, 107–112. [CrossRef]
13. Kunene, K.; Weber, M.; Sabela, M.; Voiry, D.; Kanchi, S.; Bisetty, K.; Bechelany, M. Highly-efficient electrochemical label-free immunosensor for the detection of ochratoxin A in coffee samples. *Sens. Actuators B Chem.* **2020**, *305*, 127438. [CrossRef]
14. Belbruno, J.J. Molecularly Imprinted Polymers. *Chem. Rev.* **2019**, *119*, 94–119. [CrossRef] [PubMed]
15. Chrouda, A.; Sbartai, A.; Baraket, A.; Renaud, L.; Maaref, A.; Jaffrezic-Renault, N. An aptasensor for ochratoxin A based on grafting of polyethylene glycol on a boron-doped diamond microcell. *Anal. Biochem.* **2015**, *488*, 36–44. [CrossRef] [PubMed]
16. Wei, M.; Yue, S.; Zhang, W.; Li, X. Development of an electrochemical aptasensor using Au octahedra and graphene for signal amplification. *Anal. Methods* **2020**, *12*, 317–323. [CrossRef]
17. Li, X.; Falcone, N.; Hossain, M.N.; Kraatz, H.B.; Chen, X.; Huang, H. Development of a novel label-free impedimetric electrochemical sensor based on hydrogel/chitosan for the detection of ochratoxin A. *Talanta* **2021**, *226*, 122183. [CrossRef] [PubMed]
18. Abrunhosa, L.; Paterson, R.R.M.; Venancio, A. Biodegradation of Ochratoxin A for Food and Feed Decontamination. *Toxins* **2010**, *2*, 1078–1099. [CrossRef]
19. Pitout, M. The hydrolysis of ochratoxin A by some proteolytic enzymes. *J. Biochem. Pharmacol.* **1969**, *18*, 485–491. [CrossRef]

20. Stander, M.A.; Steyn, P.S.; van der Westhuizen, F.H.; Payne, B.E. A kinetic study into the hydrolysis of the ochratoxins and analogues by carboxypeptidase A. *Chem. Res. Toxicol.* **2001**, *14*, 302–304. [CrossRef]
21. Stander, M.A.; Bornscheuer, U.T.; Henke, E.; Steyn, P.S. Screening of Commercial Hydrolases for the Degradation of Ochratoxin A. *J. Agric. Food Chem.* **2000**, *48*, 5736–5739. [CrossRef]
22. Abrunhosa, L.; Santos, L.; Venancio, A. Degradation of Ochratoxin A by Proteases and by a Crude Enzyme of Aspergillus niger. *Food Biotechnol.* **2006**, *20*, 231–242. [CrossRef]
23. Dobritzsch, D.; Wang, H.; Schneider, G.; Yu, S. Structural and functional characterization of ochratoxinase, a novel mycotoxin-degrading enzyme. *Biochem. J.* **2014**, *462*, 441–452. [CrossRef] [PubMed]
24. Hayashi, R.; Bai, Y.; Hata, T. Further Confirmation of Carboxypeptidase Y as a Metal-Free Enzyme Having a Reactive Serine Residue. *J. Biochem.* **1975**, *77*, 1313–1318. [CrossRef]
25. Dridi, F.; Marrakchi, M.; Gargouri, M.; Saulnier, J.; Jaffrezic-Renault, N.; Lagarde, F. Comparison of carboxypeptidase Y and thermolysin for ochratoxin A electrochemical biosensing. *Anal. Methods* **2015**, *7*, 8954. [CrossRef]
26. Endo, S. Studies on protease by thermophilic bacteria. *J. Ferment. Technol.* **1962**, *40*, 346–353.
27. Morihara, K.; Tsuzuki, H. Thermolysin: Kinetic Study with Oligopeptides. *J. Biochem.* **1970**, *15*, 374–380. [CrossRef] [PubMed]
28. Dridi, F.; Marrakchi, M.; Gargouri, M.; Garcia-Cruz, A.; Dzyadevych, S.; Vocanson, F.; Saulnier, J.; Jaffrezic-Renault, N.; Lagarde, F. Thermolysin entrapped in a gold nanoparticles/polymer composite for direct and sensitive conductometric biosensing of ochratoxin A in olive oil. *Sens. Actuators B Chem.* **2015**, *221*, 480–490. [CrossRef]
29. Gorton, L.; Lindgren, A.; Larsson, T.; Munteanu, F.D.; Ruzgas, T.; Gazaryan, I. Direct electron transfer between heme-containing enzymes and electrodes as basis for third generation biosensors. *Anal. Chim. Acta* **1999**, *400*, 91–108. [CrossRef]
30. Zinoubi, K.; Chrouda, A.; Soltane, R.; Al-Ghamdi, Y.O.; Garallah Almalki, S.; Osman, G.; Barhoumi, H.; Jaffrezic-Renault, N. Highly Sensitive Impedimetric Biosensor Based on Thermolysin Immobilized on a GCE Modified with AuNP-decorated Graphene for the Detection of Ochratoxin A. *Electroanalysis* **2021**, *33*, 136–145. [CrossRef]
31. ElKaoutit, M.; Naranjo-Rodriguez, I.; Manuel Dominguez, M.; Hernandez-Artiga, M.P.; Bellido-Milla, D.; Hidalgo-Hidalgo de Cisneros, J.L. A third-generation hydrogen peroxide biosensor based on Horseradish Peroxidase (HRP) enzyme immobilized in a Nafion–Sonogel–Carbon composite. *Electrochim. Acta* **2008**, *53*, 7131–7137. [CrossRef]
32. Garcia-Moreno, M.; Moreno-Conesa, M.; Rodriguez-Lopez, J.N.; Garcia-Canovas, F.; Varon, R. Oxidation of 4-tert-butylcatechol and dopamine by hydrogen peroxide catalyzed by horseradish peroxidase. *Biol. Chem.* **1999**, *380*, 689–694. [CrossRef]
33. Ramirez, E.A.; Zon, M.A.; Jara Ulloa, P.A.; Squella, J.A.; Nunez Vergara, L.; Fernandez, H. Adsorption of ochratoxin A (OTA) anodic oxidation product on glassy carbon electrodes in highly acidic reaction media: Its thermodynamic and kinetics characterization. *Electrochim. Acta.* **2010**, *55*, 771–778. [CrossRef]
34. Serra, B.; Reviejo, A.J.; Pingarron, J.M. Composite Multienzyme Amperometric Biosensors for an Improved Detection of Phenolic Compounds. *Electroanalysis* **2003**, *15*, 1737–1744. [CrossRef]
35. Alonso Lomillo, M.A.; Kauffmann, J.M.; Arcos Martinez, M.J. HRP-based biosensor for monitoring rifampicin. *Biosens. Bioelectron.* **2003**, *18*, 1165–1171. [CrossRef] [PubMed]
36. Alonso-Lomillo, M.A.; Domínguez-Renedo, O.; Ferreira-Gonçalves, L.; Arcos-Martínez, M.J. Sensitive enzyme-biosensor based on screen-printed electrodes for Ochratoxin A. *Biosens. Bioelectron.* **2010**, *25*, 1333–1337. [CrossRef]
37. Alonso-Lomillo, M.A.; Domínguez-Renedo, O.; del Torno de Román, L.; Arcos-Martínez, M.J. Horseradish peroxidase-screen printed biosensors for determination of Ochratoxin A. *Anal. Chim. Acta* **2011**, *688*, 49–53. [CrossRef] [PubMed]
38. Huynh, M.T.; Anson, C.W.; Cavell, A.C.; Stahl, S.S.; Hammes-Schiffer, S.J. Quinone 1 e^- and 2 e^-/2 H^+ Reduction Potentials: Identification and Analysis of Deviations from Systematic Scaling Relationships. *Am. Chem. Soc.* **2016**, *138*, 15903–15910. [CrossRef] [PubMed]
39. Sbartai, A.; Jaffrezic-Renault, N.; Bougard, D.; Segarra, C.; Fournier-Wirth, C.; Kang, S.; Lim, K.; An, S.S.A. Magnetic microparticle-based multimer detection system for the electrochemical detection of prion oligomers in sheep using a recyclable BDD electrode. *Microchem. J.* **2021**, *164*, 106089. [CrossRef]
40. Rahmani, A.; Jinap, S.; Soleimany, F. Validation of the procedure for the simultaneous determination of aflatoxins ochratoxin A and zearalenone in cereals using HPLC-FLD. *Food Addit. Contam. Part A* **2010**, *27*, 1683–1693. [CrossRef] [PubMed]
41. Hetemi, D.; Noël, V.; Pinson, J. Grafting of diazonium salts on surfaces: Application to biosensors. *Biosensors* **2020**, *10*, 4. [CrossRef] [PubMed]
42. Chhin, D.; Polcari, D.; Bodart-Le Guen, C.; Tomasello, G.; Cicoira, F.; Schougaard, S.B. Diazonium-Based Anchoring of PEDOT on Pt/Ir Electrodes via Diazonium Chemistry. *J. Electrochem. Soc.* **2018**, *165*, G3066–G3070. [CrossRef]
43. Nasture, A.M.; Ionete, E.I.; Lungu, F.A.; Spiridon, S.I.; Patularu, L.G. Water Quality Carbon Nanotube-Based Sensors Technological Barriers and Late Research Trends: A Bibliometric Analysis. *Chemosensors* **2022**, *10*, 161. [CrossRef]
44. Lo, M.; Pires, R.; Diaw, K.; Gningue-Sall, D.; Oturan, M.A.; Aaron, J.J.; Chehimi, M.M. Diazonium Salts: Versatile Molecular Glues for Sticking Conductive Polymers to Flexible Electrodes. *Surfaces* **2018**, *1*, 43–58. [CrossRef]
45. Zeng, Q.; Huang, X.; Ma, M. A molecularly imprinted electrochemical sensor based on polypyrrole/carbon nanotubes composite for the detection of S-ovalbumin in egg white. *Int. J. Electrochem. Sci.* **2017**, *12*, 3965–3981. [CrossRef]
46. Lakhin, A.V.; Tarantul, V.Z.; Gening, L.V. Aptamers: Problems, solutions and prospects. *Acta Nat.* **2013**, *5*, 34–43. [CrossRef]
47. Walter, J.G.; Heilkenbrinker, A.; Austerjost, J.; Timur, S.; Stahl, F.; Scheper, T. Aptasensors for small molecule detection. *Z. Nat. Sect. B J. Chem. Sci.* **2012**, *67*, 976–986. [CrossRef]

48. Bonel, L.; Vidal, J.C.; Duato, P.; Castillo, J.R. Ochratoxin A nanostructured electrochemical immunosensors based on polyclonal antibodies and gold nanoparticles coupled to the antigen. *Anal. Methods* **2010**, *2*, 335–341. [CrossRef]
49. Zamfir, L.G.; Geana, I.; Bourigua, S.; Rotariu, L.; Bala, C.; Errachid, A.; Jaffrezic-Renault, N. Highly sensitive label-free immunosensor for ochratoxin A based on functionalized magnetic nanoparticles and EIS/SPR detection. *Sens. Actuators B Chem.* **2011**, *159*, 178–184. [CrossRef]
50. Wei, M.; Zhang, W. The determination of Ochratoxin A based on the electrochemical aptasensor by carbon aerogels and methylene blue assisted signal amplification. *Chem. Cent. J.* **2018**, *12*, 45. [CrossRef]
51. Zhang, X.; Zhi, H.; Zhu, M.; Wang, F.; Meng, H.; Feng, L. Electrochemical/visual dual-readout aptasensor for Ochratoxin A detection integrated into a miniaturized paper-based analytical device. *Biosens. Bioelectron.* **2021**, *180*, 113146. [CrossRef] [PubMed]
52. Ni, X.; Zhang, Y.; Xue, C.; Chen, X. Ultrasensitive Detection of Ochratoxin A with a Zeolite Imidazolate Frameworks Composite–Based Electrochemical Aptasensor. *Front. Chem.* **2022**, *10*, 858107. [CrossRef] [PubMed]
53. Mazaafrianto, D.N.; Ishida, A.; Maeki, M.; Tani, H.; Tokeshi, M. Label-Free Electrochemical Sensor for Ochratoxin A Using a Microfabricated Electrode with Immobilized Aptamer. *ACS Omega* **2018**, *3*, 16823–16830. [CrossRef]
54. Lv, L.; Li, D.; Liu, R.; Cui, C.; Guo, Z. Label-free aptasensor for ochratoxin A detection using SYBR gold as a probe. *Sens. Actuators B Chem.* **2017**, *246*, 647–652. [CrossRef]